MV^{2+}. Likewise, Tris–HCl buffer (25 mM, pH 7.5 with 100 mM KCl) solutions of GroEL–CdS complex and *T.th* cpn–CdS complex (2 ml, 700 nm based on Cd^{2+}) were titrated. Emission ($\lambda_{ext} = 370$ nm) spectra were recorded on a FP-777W spectrophotometer (JASCO).

Thermal stability

Fluorescence spectra ($\lambda_{ext} = 370$ nm, wavelength of observed fluorescence $\lambda_{obsd} = 530$ nm) of GroEL–CdS complexes and *T.th* cpn–CdS complexes were recorded at designated temperatures on a FP-777W spectrophotometer (JASCO), where the fluorescence intensities at 4 °C were used as the bases for relative fluorescence intensities. The temperature was directly controlled by a ECT271 Peltier thermometric apparatus (JASCO; 40 °C min^{-1} on heating and 25 °C min^{-1} on cooling).

ATP response

To a 2-ml Tris–HCl buffer (25 mM, pH 7.5 with 100 mM KCl) solution of *T.th* cpn–CdS complexes (0.5 μM based on *T.th* cpn) were added aqueous solutions of ATP (100 mM) and $MgCl_2$ (1 M) ([ATP] = 20 μM, $[Mg^{2+}] = 25$ mM after mixing), and the mixture was incubated at 70 °C for 10 min. The supernatant solution was subjected to fluorescence spectroscopy and analytical SEC with an UV/fluorescence dual detector.

Received 11 November 2002; accepted 14 April 2003; doi:10.1038/nature01663.

1. Alivisatos, A. P. Semiconductor clusters, nanocrystals, and quantum dots. *Science* **271,** 933–937 (1996).
2. Schmid, G. *et al.* Current and future applications of nanoclusters. *Chem. Soc. Rev.* **28,** 179–185 (1999).
3. Meldrum, F. C., Heywood, B. R. & Mann, S. Magnetoferritin — *in vitro* synthesis of a novel magnetic protein. *Science* **257,** 522–523 (1992).
4. Wong, K. K. W. & Mann, S. Biomimetic synthesis of cadmium sulfide-ferritin nanocomposites. *Adv. Mater.* **8,** 928–932 (1996).
5. Shenton, W., Pum, D., Sleytr, U. B. & Mann, S. Biocrystal templating of CdS superlattices using self-assembled bacterial S-layers. *Nature* **389,** 585–587 (1997).
6. Balogh, L. & Tomalia, D. A. Poly(amidoamine) dendrimer-templated nanocomposites. 1. Synthesis of zerovalent copper nanoclusters. *J. Am. Chem. Soc.* **120,** 7355–7356 (1998).
7. Lemon, B. I. & Crooks, R. M. Preparation and characterization of dendrimer-encapsulated CdS semiconductor quantum dots. *J. Am. Chem. Soc.* **122,** 12886–12887 (2000).
8. Shenton, W., Mann, S., Cölfen, H., Bacher, A. & Fischer, M. Synthesis of nanophase iron oxide in lumazine synthase capsids. *Angew. Chem. Int. Edn Engl.* **40,** 442–445 (2001).
9. McMillan, R. A. *et al.* Ordered nanoparticle arrays formed on engineered chaperonin protein templates. *Nature Mater.* **1,** 247–252 (2002).
10. Roseman, A. M., Chen, S., White, H., Braig, K. & Saibil, H. R. The chaperonin ATPase cycle: mechanism of allosteric switching and movements of substrate-binding domains in groEL. *Cell* **87,** 241–251 (1996).
11. Ranson, N. A. *et al.* ATP-bound states of groEL captured by cryo-electron microscopy. *Cell* **107,** 869–879 (2001).
12. Hendrix, R. W. Purification and properties of groE, a host protein involved in bacteriophage assembly. *J. Mol. Biol.* **129,** 375–392 (1979).
13. Braig, K. *et al.* The crystal structure of the bacterial chaperonin groEL at 2.8 Å. *Nature* **371,** 578–586 (1994).
14. Taguchi, H., Konishi, J., Ishii, N. & Yoshida, M. A chaperonin from a thermophilic bacterium, *Thermus thermophilus*, that controls refoldings of several thermophilic enzymes. *J. Biol. Chem.* **266,** 22411–22418 (1991).
15. Amada, K. *et al.* Molecular cloning, expression, and characterization of chaperonin-60 and chaperonin-10 from a thermophilic bacterium, *Thermus thermophilus* HB8. *J. Biochem.* **118,** 347–354 (1995).
16. Ishii, N., Taguchi, H., Sumi, M. & Yoshida, M. Structure of holo-chaperonin studied with electron microscopy. Oligomeric cpn10 on top of two layers of cpn60 rings with two stripes each. *FEBS Lett.* **299,** 169–174 (1992).
17. Ishii, N., Taguchi, H., Sasabe, H. & Yoshida, M. Folding intermediate binds to the bottom of bullet-shaped holo-chaperonin and is readily accessible to antibody. *J. Mol. Biol.* **236,** 691–696 (1994).
18. Murakoshi, K. *et al.* Preparation of size-controlled hexagonal CdS nanocrystallites and the characteristics of their surface structures. *J. Chem. Soc. Faraday Trans.* **94,** 579–586 (1998).
19. Hosokawa, H. *et al. In-situ* EXAFS observation of the surface structure of colloidal CdS nanocrystallites in *N*,*N*-dimethylformamide. *J. Phys. Chem.* **100,** 6649–6656 (1996).
20. Brus, L. E. Electron-electron and electron-hole interactions in small semiconductor crystallites: The size dependence of the lowest excited electronic state. *J. Chem. Phys.* **80,** 4403–4409 (1984).
21. Ramsden, J. J. & Grätzel, M. Photoluminescence of small cadmium sulfide particles. *J. Chem. Soc. Faraday Trans. 1* **80,** 919–933 (1984).
22. Hengleln, A. Photochemistry of colloidal cadmium sulfide. 2. Effects of adsorbed methyl viologen and of colloidal platinum. *J. Phys. Chem.* **86,** 2291–2293 (1982).
23. Llorca, O., Galán, A., Carrascosa, J. L., Muga, A. & Valpuesta, J. M. GroEL under heat-shock. *J. Biol. Chem.* **273,** 32587–32594 (1998).
24. Martin, J., Horwich, A. L. & Hartl, F. U. Prevention of protein denaturation under heat stress by the chaperonin Hsp60. *Science* **258,** 995–998 (1992).
25. Goloubinoff, P., Christeller, J. T., Gatenby, A. A. & Lorimer, G. H. Reconstitution of active dimeric ribulose bisphosphate carboxylase from an unfolded state depends on two chaperonin proteins and Mg-ATP. *Nature* **342,** 884–889 (1989).
26. Todd, M. J., Viitanen, P. V. & Lorimer, G. H. Hydrolysis of adenosine 5′-triphosphate by *Escherichia coli* groEL: effects of groES and potassium ion. *Biochemistry* **32,** 8560–8567 (1993).

Supplementary Information accompanies the paper on **www.nature.com/nature**.

Acknowledgements We thank K. Konishi for his initial contribution to the present work; K. Tsumoto for discussions; J. Oono and M. Nakamura for SEC analysis with MALS. N.I. was responsible for TEM microscopy. We acknowledge support from the 21st Century COE Programs of Research and Education (T.A., Human–Friendly Materials Based on Chemistry; M.Y., Future Nano-Materials), and from the JST ERATO Nanospace program. K.K. acknowledges support from the Nissan Science Foundation.

Competing interests statement The authors declare that they have no competing financial interests.

Correspondence and requests for materials should be addressed to T.A. (aida@macro.t.u-tokyo.ac.jp).

Evidence for low sulphate and anoxia in a mid-Proterozoic marine basin

Yanan Shen*, Andrew H. Knoll* & Malcolm R. Walter†

** Botanical Museum, Harvard University, 26 Oxford Street, Cambridge, Massachusetts 02138, USA*
† Australian Centre for Astrobiology, Macquarie University, New South Wales 2109, Australia

Many independent lines of evidence document a large increase in the Earth's surface oxidation state 2,400 to 2,200 million years ago[1–4], and a second biospheric oxygenation 800 to 580 million years ago, just before large animals appear in the fossil record[5,6]. Such a two-staged oxidation implies a unique ocean chemistry for much of the Proterozoic eon, which would have been neither completely anoxic and iron-rich as hypothesized for Archaean seas, nor fully oxic as supposed for most of the Phanerozoic eon[7]. The redox chemistry of Proterozoic oceans has important implications for evolution[8], but empirical constraints on competing environmental models are scarce. Here we present an analysis of the iron chemistry of shales deposited in the marine Roper Basin, Australia, between about 1,500 and 1,400 million years ago, which record deep-water anoxia beneath oxidized surface water. The sulphur isotopic compositions of pyrites in the shales show strong variations along a palaeodepth gradient, indicating low sulphate concentrations in mid-Proterozoic oceans. Our data help to integrate a growing body of evidence favouring a long-lived intermediate state of the oceans, generated by the early Proterozoic oxygen revolution and terminated by the environmental transformation late in the Proterozoic eon.

The Roper Group is a thick (>1,500 m), predominately marine siliciclastic succession preserved over an area of 145,000 km^2 west of the Gulf of Carpenteria in Australia's Northern Territory. The ramp-like succession, formed in an intracratonic basin in contact with the global ocean, contains six major depositional sequences that record episodic flooding followed by basin filling and shoreline progradation[9]. Facies are laterally persistent and repeat vertically in successive sequences, allowing environmental variations in seawater chemistry to be distinguished from long-term secular changes. Zircons from a tuff low in the succession have yielded a U–Pb sensitive high-resolution ion microprobe age of 1,492 ± 3 Myr[9]. Our samples were collected from four drill cores (Urapunga 4, 5; Amoco 82/3; Golden Grove 1) (Fig. 1): there were a total of 117 samples—37 from inner-shelf shales, 37 from distal-shelf facies, and 43 from basinal environments, as interpreted[9] using sedimentological criteria.

To investigate the redox chemistry of the Roper seaway, we examined Fe species—including dithionite-extractable Fe (Fe_D), pyrite Fe (Fe_P), HCl-extractable Fe (Fe_H), and total Fe (Fe_T)—in carbonaceous shales. Two ratios, that between highly reactive Fe

($Fe_{HR} = Fe_D + Fe_P$) and Fe_T, and the ratio $Fe_P/(Fe_P + Fe_H)$, known as the degree of pyritization (DOP), have been used successfully to evaluate the redox state of ancient oceans[10–13]. DOP < 0.45 and $Fe_{HR}/Fe_T < 0.38$ are generally found for sediments depositing from oxic bottom water, whereas DOP > 0.45 and $Fe_{HR}/Fe_T > 0.38$ may be diagnostic for euxinic sediments[10,12]. The enrichment of Fe_{HR} and high DOP in euxinic sediments arises fundamentally from pyrite formation in the upper zone of the sulphidic water column, where dissolved iron concentrations can be high[10,13]. The extra reactive iron in euxinic water columns originates primarily from the reduction of iron oxides in basin margin sediments that can be transported to the ocean interior, or from iron oxide containing particles falling through the water column[12–13]. In contrast, when bottom waters are oxygenated, pyrite can only form where anoxic conditions become established within the sediment[10]. Consequently, because water-column Fe scavenging is absent, oxic marine sediments are characterized by low Fe_{HR}/Fe_T and DOP values[10,12].

Roper shales from inner-shelf environments have low Fe_{HR}/Fe_T (0.03–0.18; mean 0.07) and low DOP (0.00–0.34; mean 0.12). Similarly, Fig. 1 shows that Fe_{HR}/Fe_T and DOP for most distal-shelf shales fall within the 'oxic' quadrant defined by $Fe_{HR}/Fe_T < 0.38$ and DOP < 0.45 (full analytical data are available as Supplementary Information). In contrast, basinal sediments are dominated by high Fe_{HR}/Fe_T (>0.38) and DOP (>0.45) values, indicating euxinic bottom waters (Fig. 1; see also ref. 14). The relatively low Fe_{HR}/Fe_T and DOP in some basinal shales of the Roper Group could result from the decreased transfer of dissolved Fe from shelf sediments or from a high flux of terrestrial clastics[12,13]. Alternatively, it may be that anoxia was established at depths greater than the shelf–basin boundary (defined in ref. 9 on the basis of physical sedimentary features). Regardless, high DOP and Fe_{HR}/Fe_T together provide compelling evidence for the presence of predominantly euxinic deep waters beneath oxic surface waters at the time that Roper sediments were deposited.

We measured the S isotopic compositions of sedimentary pyrites along the same palaeoenvironmental gradient from inner-shelf to deep basinal facies. Although the literature is replete with data showing stratigraphic variation in the S isotopic compositions of sedimentary pyrite, the data presented here are, to the best of our knowledge, the first to be integrated fully with the sequence stratigraphy of a Proterozoic basin, allowing us to understand how biogeochemical data correlate with environmental setting. The total range of variation among Roper pyrites is about 70‰, similar to many Phanerozoic basins[7,15,16]. In the Roper basin, however, no one facies displays the full range of variation observed for the succession as a whole. Rather, as shown in Fig. 2, different sedimentary facies along the onshore–offshore gradient exhibit consistent differences in $\delta^{34}S$, with the most negative values occurring in basinal shales and the most positive in inner-shelf samples.

Figure 3 shows more clearly the nature and origin of these facies differences. Basinal samples exhibit a wide spread of $\delta^{34}S$ values, from +20 to +25.5‰ that approximate the isotopic composition of sulphate in Roper seawater[17] to values as negative as −20.7‰ that match the maximum fractionation directly associated with dissimilatory sulphate reduction (~45‰)[3,16]. Note, however, that strong fractionation is evident only in samples whose Fe speciation data indicate euxinic deposition.

In the presence of non-limiting sulphate (perhaps 1 mM, but possibly less), pure cultures and natural populations of sulphate-reducing bacteria fractionate sulphur isotopes strongly, up to 45‰ (refs 3, 16). The marked ^{34}S depletion in basinal samples are thus consistent with pyrite deposition from seawater sulphate with an S isotopic value of +20‰ to +25‰ (ref. 17). In this interpretation, both anoxia and the ready availability of sulphate characterize basinal waters most likely to have been in direct contact with the global ocean. Within underlying sediments, however, low diffusion rates and high bacterial sulphate demand can deplete supplies of sulphate, with a concomitant reduction in fractionation[18], explaining the few strongly positive $\delta^{34}S$ values for basinal sediments in our study (Fig. 2) and in highly organic-rich shales of the Velkerri Formation[19].

Shallower basinal, distal shelf, and most proximal shelf samples display a consistent range of variation between about +10.2‰ and +27.6‰ (Fig. 2). Strongly positive $\delta^{34}S$ values, up to +49.7‰, are restricted to shales in coastal environment. The same pattern of facies variation is seen whether one compares similar stratigraphic intervals in different parts of the basin (Urapunga 4 and Golden Grove 1) or different stratigraphic intervals (Urapunga 4 and 5) (Fig. 3). Given the iron speciation chemistry of these samples, shelf pyrites must have formed within organic-rich sediments during early diagenesis. Within sediments, sulphate abundance can become limited by diffusion and as a result, $\delta^{34}S$ values of early diagenetic pyrites commonly span the full range with strong to essentially no fractionation relative to seawater sulphate[12,15]. For example, in the modern Black Sea, with a sulphate concentration of about 20 mM, maximum S isotopic fractionations between sedimentary pyrites and seawater sulphate from estuarine, oxic shelf, and euxinic deep-

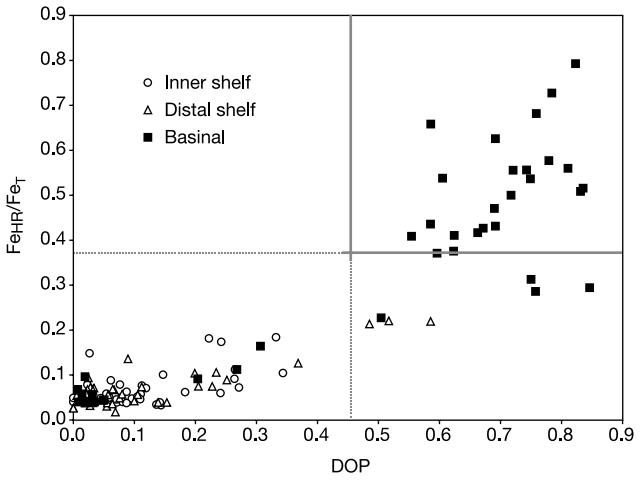

Figure 1 The relationship between the Fe_{HR}/Fe_T ratio and DOP in black shales of the Roper Group. The vertical and horizontal lines cross at a DOP value of 0.45 and a Fe_{HR}/Fe_T ratio of 0.38. In modern marine environments, samples with DOP and Fe_{HR}/Fe_T above these values (within the quadrant enclosed by solid lines) deposit beneath euxinic waters.

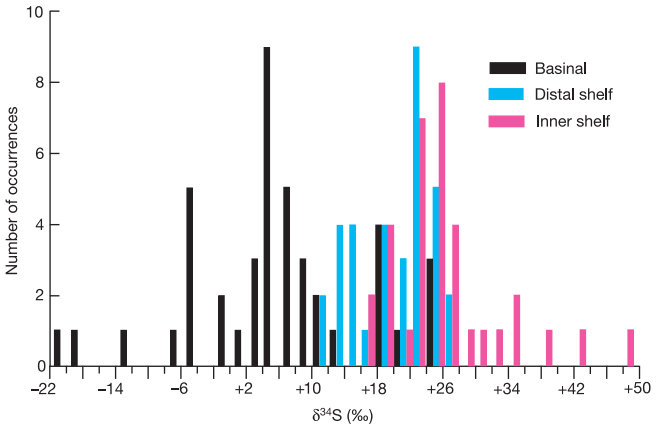

Figure 2 The S isotopic composition of sedimentary pyrites from Roper black shales. Note that samples from different environments form coherent suites. Black, basinal facies; green, distal shelf; pink, inner shelf. $\delta^{34}S$ in ‰ = $[(^{34}S/^{32}S)_{sample}/(^{34}S/^{32}S)_{standard} - 1] \times 1000$ relative to the Cañon Diablo Troilite standard.

sea sediments are comparable in magnitude, but oxic environments record a much greater range of values[13,20].

The same is true for Phanerozoic examples. Gauthier[21] measured $\delta^{34}S$ values for pyrites deposited beneath oxic and anoxic bottom waters of the Cretaceous seas that flooded North America. Like our Roper samples, Cretaceous pyrites from anoxic environments are highly ^{34}S-depleted with strong fractionations relative to seawater sulphate. Unlike the Roper samples, however, most Cretaceous pyrites that formed within sediments beneath oxic waters are also significantly depleted in ^{34}S with marked fractionations relative to sulphate. The probability that the Roper shelf pyrites were drawn from a sample with a distribution of $\delta^{34}S$ values like the Cretaceous seaway is vanishingly small ($P < 0.001$; Kolmogorov–Smirnov test).

The observed palaeoenvironmental gradient of S isotopic compositions (Fig. 2) is consistent with previous hypotheses of a sulphate-minimum zone in a stratified Proterozoic ocean[22]; such zonation could occur only if marine sulphate levels were low[22]. Under these conditions, we would expect ^{34}S-enrichment of sulphate within the sulphate-minimum zone, leading to the formation of ^{34}S-enriched sulphides, as observed in Roper shelf samples (Fig. 2). Moreover, in an inner-shelf area, high rates of primary production and rapid sedimentation would further have exaggerated the consequences of low sulphate levels. Particularly under conditions of low sulphate abundance, sulphate removal by bacteria would have outstripped rates of sulphate supply, producing porewater sulphate (and, in consequence, sulphides) with $\delta^{34}S$ values much heavier than mean seawater sulphate[15,16] (Fig. 2). It is hard to produce explanations for the observed facies dependence of S isotopic compositions (Fig. 2) that do not require sea water with sulphate concentrations far below those seen today.

Individual basins need not mirror the chemistry of the oceans as a whole. Therefore, data from other basins are needed to choose unequivocally between local and global interpretations of basinal anoxia and sulphate concentration. Fe speciation data and strongly ^{34}S-enriched pyrites from black shales deposited during maximum flooding of the Tawallah and McArthur basins (about 1,730 Myr and 1,637 Myr ago, respectively), both antecedent to Roper deposition in northern Australia, show deep-water anoxia as well as moderate-to-pronounced sulphate depletion[12]. Thus, in this one area of the world, low sulphate and basinal euxinic conditions were present in three successive basins spanning more than 250 million years of Proterozoic Earth history.

The high $\delta^{34}S$ values of disseminated pyrite in broadly contemporaneous (~1,470–1,440 Myr ago) shales of the Newland Formation, Lower Belt Supergroup, Montana, also indicate sulphate limitation[23]. The Belt Basin may have been partially isolated from the global ocean, but more highly fractionated S in pyrites ($\delta^{34}S = -14‰$ to $+18‰$) from the upper Newland Formation suggests at least episodic connection of Belt waters to the Proterozoic ocean[24]. $\delta^{34}S$ values of bedded $CaSO_4$ evaporites from a ~1,200-Myr-old carbonate-evaporite succession in northern Canada vary markedly with stratigraphy; this variation could be explained as follows. Where seawater sulphate levels were low, $\delta^{34}S$ values for sulphate varied as a function of sulphate removal by bacterial sulphate reduction and consequent iron sulphide precipitation[25]. In contrast to the Phanerozoic record, positive $\delta^{34}S$ values characterize early diagenetic pyrites from mid-Proterozoic shelf shales around the world[15,16], consistent with low sulphate throughout the world's oceans. Limited data suggest that marine sulphate levels may have remained low until near the end of the Proterozoic eon[26].

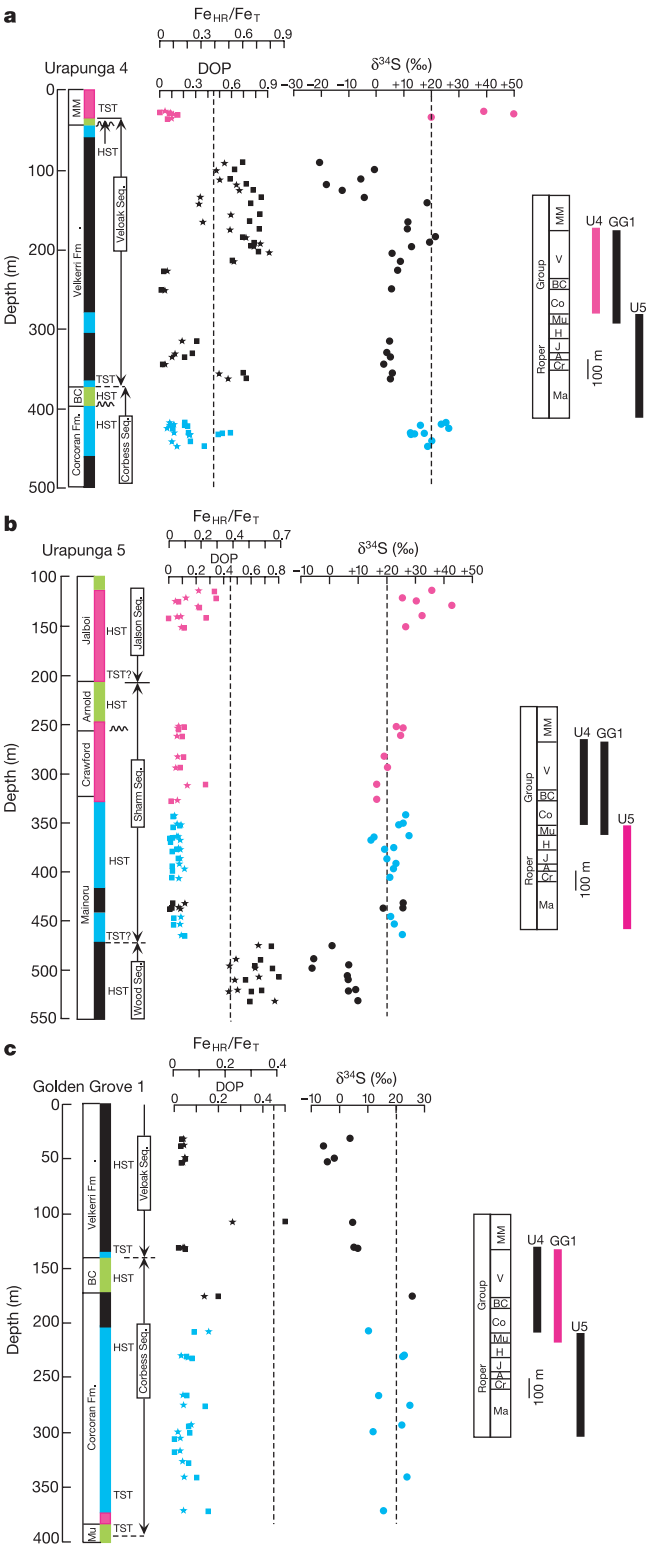

◀ **Figure 3** Fe-speciation, S-isotopic, and sequence-stratigraphic data for the Roper Group. Panels **a**–**c** show data obtained from three drilling sites: **a**, Urapunga 4; **b**, Urapunga 5; **c**, Golden Grove 1. +20‰ represents the possible isotopic composition of open seawater sulphate for middle Proterozoic. In each panel, the left-hand dashed line is drawn at a DOP value of 0.45 (with DOP data shown as filled squares) and an Fe_{HR}/Fe_T ratio of 0.38 (stars). Sequence stratigraphy is from ref. 9. On the right side of each panel, stratigraphy of the Roper Group shows intervals intersected by the drill cores of Urapunga 4 (U4), POG Golden Grove 1 (GG1) and BMR Urapunga 5 (U5). MM, McMinn Formation; V, Velkerri Formation; BC, Bessie Creek Sandstone; Co, Corcoran Formation; Mu, Munyi Member; H, Hodgson Sandstone; J, Jalboi Formation; A, Arnold Sandstone; Cr, Crawford Formation; Ma, Mainoru Formation. Black, basinal facies; green, distal shelf; pink, inner shelf; olive, estuarine. TST, Transgressive Systems Tract; HST, Highland Systems Tract.

The documentation of euxinic and low sulphate conditions in mid-Proterozoic marine basins paves the way to an improved understanding of early life and environments. In such oceans, methanogenic archaeans could have played an enhanced role in the carbon cycle, contributing to long-lived greenhouse conditions[27]. Low sulphate may also help to explain the prominence of penecontemporaneous dolomite in mid-Proterozoic and older carbonate platforms[28]. Through its effects on biologically important trace elements, seawater chemistry may help to explain the ecological and evolutionary distributions of early eukaryotic photoautotrophs[8]. And, if sulphate levels remained low until the latest Proterozoic, oxygen probably also remained well below present levels, influencing the early diversification of animals[29]. Further biogeochemical research carried out in the framework of sequence stratigraphy[30] should clarify the relationships between seawater chemistry and changes in the Proterozoic biosphere. □

Received 14 November 2002; accepted 10 April 2003; doi:10.1038/nature01651.

1. Holland, H. D. in *Early Life on Earth* (ed. Bengtson, S.) 237–244 (Columbia Univ. Press, New York, 1994).
2. Farquhar, J., Bao, H. & Thiemans, M. H. Atmospheric influence of the Earth's earliest sulphur cycle. *Science* **289,** 756–758 (2000).
3. Canfield, D. E., Habicht, K. S. & Thamdrup, B. The Archean sulfur cycle and the early history of atmospheric oxygen. *Science* **288,** 658–661 (2000).
4. Des Marais, D. J., Strauss, H., Summons, R. E. & Hayes, J. M. Carbon isotopic evidence for the stepwise oxidation of the Precambrian environment. *Nature* **359,** 605–609 (1992).
5. Derry, L. A., Kaufman, A. J. & Jacobsen, S. B. Sedimentary cycling and environmental change in the late Proterozoic: evidence from stable and radiogenic isotopes. *Geochim. Cosmochim. Acta* **56,** 1317–1329 (1992).
6. Canfield, D. E. & Teske, A. Late Proterozoic rise in atmospheric oxygen concentrations inferred from phylogenetic and stable-isotope studies. *Nature* **382,** 127–132 (1996).
7. Canfield, D. E. A new model for Proterozoic ocean chemistry. *Nature* **396,** 450–453 (1998).
8. Anbar, A. D. & Knoll, A. H. Proterozoic ocean chemistry and evolution: A bioinorganic bridge? *Science* **297,** 1137–1142 (2002).
9. Abbott, S. T. & Sweet, I. P. Tectonic control on third-order sequences in a siliciclastic ramp-style basin: an example from the Roper Superbasin (Mesoproterozoic), northern Australia. *Aust. J. Earth Sci.* **47,** 637–657 (2000).
10. Raiswell, R. & Canfield, D. E. Sources of iron for pyrite formation in marine sediments. *Am. J. Sci.* **298,** 219–245 (1998).
11. Raiswell, R., Newton, R. & Wignall, P. B. An indicator of water-column anoxia: resolution of biofacies variations in the Kimmeridge clay (upper Jurassic, U.K.). *J. Sedim. Res.* **71,** 286–294 (2001).
12. Shen, Y., Canfield, D. E. & Knoll, A. H. Middle Proterozoic ocean chemistry: Evidence from the McArthur Basin, northern Australia. *Am. J. Sci.* **302,** 81–109 (2002).
13. Wijsman, J. W. M., Middelburg, J. J., Herman, P. M. J., Böttcher, M. E. & Heip, C. H. R. Sulfur and iron speciation in surface sediments along the northwestern margin of the Black Sea. *Mar. Chem.* **74,** 261–278 (2001).
14. Jackson, M. J. & Raiswell, R. Sedimentology and carbon-sulphur geochemistry of the Velkerri Formation, a mid-Proterozoic potential oil source in northern Australia. *Precambr. Res.* **54,** 81–108 (1991).
15. Hayes, J. M., Lambert, I. B. & Strauss, H. in *The Proterozoic Biosphere: A Multidisciplinary Study* (eds Schopf, J. W. & Klein, C.) 129–134 (Cambridge Univ. Press, Cambridge, 1992).
16. Canfield, D. E. & Raiswell, R. The evolution of the sulfur cycle. *Am. J. Sci.* **299,** 697–723 (1999).
17. Muir, M. D., Donnelly, T. H., Wilkins, R. W. T. & Armstrong, K. J. Stable isotope, petrological, and fluid inclusion studies of minor mineral deposits from the McArthur Basin: implications for the genesis of some sediment-hosted base metal mineralization from the Northern Territory. *Aust. J. Earth Sci.* **32,** 239–260 (1985).
18. Zaback, D. A., Pratt, L. M. & Hayes, J. M. Transport and reduction of sulfate and immobilization of sulfide in marine black shales. *Geology* **21,** 141–144 (1993).
19. Donnelly, T. H. & Crick, I. H. Depositional environment of the middle Proterozoic Velkerri Formation in northern Australia: geochemical evidence. *Precambr. Res.* **42,** 165–172 (1988).
20. Lyons, T. W. Sulfur isotopic trends and pathways of iron sulphide formation in upper Holocene sediments of the anoxic Black Sea. *Geochim. Cosmochim. Acta* **61,** 3367–3382 (1997).
21. Gautier, D. Cretaceous shales from the western interior of North America: sulfur/carbon ratios and sulfur isotope composition. *Geology* **14,** 225–228 (1986).
22. Logan, G. A., Hayes, J. M., Hieshima, G. B. & Summons, R. E. Terminal Proterozoic reorganization of biogeochemical cycles. *Nature* **376,** 53–56 (1995).
23. Lyons, T. W., Luepke, J. J., Schreiber, M. E. & Zeig, G. A. Sulfur geochemical constraints on Mesoproterozoic restricted marine deposition: lower Belt Supergroup, northwestern United States. *Geochim. Cosmochim. Acta* **64,** 427–437 (2000).
24. Strauss, H. & Schieber, J. A sulfur isotope study of pyrite genesis: The Mid-Proterozoic Newland Formation, Belt Supergroup, Montana. *Geochim Cosmochim Acta* **54,** 197–204 (1990).
25. Kah, L. C., Lyons, T. W. & Chesley, J. T. Geochemistry of a 1.2 Ga carbonate-evaporite succession, northern Baffin and Bylot Islands: implications for Mesoproterozoic marine evolution. *Precambr. Res.* **111,** 203–234 (2001).
26. Hurtgen, M. T., Arthur, M. A., Suits, N. S. & Kaufman, A. J. The sulfur isotopic composition of Neoproterozoic seawater sulfate: implications for a snowball Earth? *Earth Planet. Sci. Lett.* **203,** 413–429 (2002).
27. Pavlov, A. A., Hurtgen, M. T., Kasting, J. F. & Arthur, M. A. Methane-rich Proterozoic atmosphere? *Geology* **31,** 87–90 (2003).
28. Baker, P. A. & Kastner, M. Constraints on the formation of sedimentary dolomite. *Science* **213,** 214–216 (1981).
29. Knoll, A. H. & Carroll, S. B. Early animal evolution: emerging views from comparative biology and geology. *Science* **284,** 2129–2137 (1999).
30. Ross, G. M., Bloch, J. D. & Krouse, H. R. Neoproterozoic strata of the southern Canadian Cordillera and the isotopic evolution of seawater sulfate. *Precambr. Res.* **73,** 71–99 (1995).

Supplementary Information accompanies the paper on **www.nature.com/nature**.

Acknowledgements We thank A. Bauer and J. Brocks for help in sample collection, J. Fong and L. Liu for help with geochemical analysis, J. Payne for help with statistics, and D. Canfield, J. Hayes, M. Hurtgen, T. Lyons and G. Ross for comments and suggestions. This study was supported by an NRC Research Associateship (Y.S.), the NASA Exobiology programme, the Astrobiology Institute, Macquarie University, and the Australian Research Council.

Competing interests statement The authors declare that they have no competing financial interests.

Correspondence and requests for materials should be addressed to Y.S. (yshen@oeb.harvard.edu).

Stability of forest biodiversity

James S. Clark & Jason S. McLachlan

Center on Global Change, Biology, and Nicholas School of the Environment, Duke University, Durham, North Carolina 27708, USA

Two hypotheses to explain potentially high forest biodiversity have different implications for the number and kinds of species that can coexist and the potential loss of biodiversity in the absence of speciation. The first hypothesis involves stabilizing mechanisms, which include tradeoffs between species in terms of their capacities to disperse to sites where competition is weak[1–4], to exploit abundant resources effectively[5,6] and to compete for scarce resources[7]. Stabilization results because competitors thrive at different times and places. An alternative, 'neutral model' suggests that stabilizing mechanisms may be superfluous. This explanation emphasizes 'equalizing' mechanisms[8], because competitive exclusion of similar species is slow. Lack of ecologically relevant differences means that abundances experience random 'neutral drift', with slow extinction[9–11]. The relative importance of these two mechanisms is unknown, because assumptions and predictions involve broad temporal and spatial scales. Here we demonstrate that predictions of neutral drift are testable using palaeodata. The results demonstrate strong stabilizing forces. By contrast with the neutral prediction of increasing variance among sites over time, we show that variances in post-Glacial tree abundances among sites stabilize rapidly, and abundances remain coherent over broad geographical scales.

It is difficult to test competing hypotheses for coexistence. In ecological models, stable coexistence typically requires tradeoffs. Communities may be 'packed', in the sense that only species with particular life history combinations can coexist[3]. The potential importance of stabilizing forces has led to searches for tradeoffs that partition advantages in space and time between different species[12]. Although some types of tradeoffs are clear-cut, such as those characterizing early and late successional species[13,14], the overall importance of tradeoffs is debatable[10,12,15].

By contrast, if species differences are small, the inherent limits to diversity implied by specific types of competition may not apply. The neutral model does not refer to a strict random walk, because finite space limits the density of trees. Rather, ecological equivalence allows that abundances drift randomly. Speciation might balance losses, provided that new species are generated as rapidly as random extinction removes them. Although there are unique temporal patterns associated with processes such as random drift, for trees